IOSR Journal of Electronics and Communication Engineering (IOSR-JECE)
e-ISSN: 2278-2834,p- ISSN: 2278-8735.Volume 17, Issue 5, Ser. I (Sep. – Oct. 2022), PP 15-26
www.iosrjournals.org

Study the performance of GeSn/SiGeSn quantum well infrared photodetector on silicon-on-insulator in mid-infrared region

Soumava Ghosh
Institute of Radio Physics and Electronics, University of Calcutta, 92 A. P. C Road, Kolkata-700009

Abstract
Quantum well infrared photodetectors (QWIPs) have attracted researchers due to their high absorption coefficient at longer wavelength, low noise, high operational speed and high infrared sensitivity. In this work the author has proposed an intersubabnd GeSn/SiGeSn QWIP on a silicon-on-insulator (SOI) substrate. The top SiO_2 anti-reflection layer and bottom buried oxide layer create vertical cavity effect that considerably increased the light-matter interaction inside the QWIP and thereby the optical response. After that different theoretical approaches have been discussed to increase the 3-dB bandwidth (BW) of the QWIP without compromising detectivity. This work suggests that the proposed GeSn/SiGeSn QWIPs on SOI are an encouraging contender for higher 3-dB BW along with high detectivity in mid infrared region for optical detection.

Keywords*: Mid-infrared, photodetectors, 3-dB Bandwidth, Responsivity, Detectivity.*

Date of Submission: 05-09-2022 Date of Acceptance: 19-09-2022

I. Introduction

Nowadays, mid-infrared (MIR) range [3-5 μm] has attracted researchers because of its different notable applications such as spectroscopic sensing, materials processing, chemical and biomolecular sensing, security, surveillance. Apart from those applications the MIR region also covers the sensing wavelengths of different toxic gasses including CO, CO_2, CH_4, HF, H_2S [1]. Therefore, the continuous increase of applications of MIR wavelength demands suitable photodetectors (PDs) with high infrared (IR) sensibility and matured fabrication. Over last few decades beyond telecommunication application different narrow bandgap semiconductor-based PDs have shown very encouraging performance in the MIR wavelength range. Among them researchers have been attracted by quantum well infrared photodetectors (QWIPs) due to their physical characteristics and important practical applications in medical imaging, optical communication, spectroscopic sensing [2-6]. Since last 30 years several group of researchers have reported their theoretical and experimental analysis of group III-V-based QWIPs [2,3,7-14].

Nowadays, Si-Photonics is emerging as a platform of electronic-photonic integrated circuits (EPICs) due to their cheap and mature fabrication, high IR sensibility and high operational speed. The integrated QWIP is one of the important units of the EPICs [15]. In spite of the promising performance of commercially available III-V-based QWIPs [2,3,7-14], their incompatibility with Si-based complementary-metal-oxide-semiconductor (CMOS) processing technology increases the fabrication cost as well as restricts large scale integration. Alternatively, SiGe/Si-based QWIPs operated in MIR region have drawn attraction due to their compatibility with Si-based CMOS processing technology and monolithic integration on a same Si chip [16-21]. However, the large number of nonradiative recombination centres and high lattice mismatch between Ge and Si interface (> 4%) have limited their performance far below than the III-V-based QWIPs [16,19-21].

In last two decades the successful growth of high-quality $Ge_{1-x}Sn_x$ thin films on Si substrate via a suitable buffer layer using chemical vapour deposition [22,23] and molecular beam epitaxy [24] have changed the scenario completely. Incorporation of α-Sn into Ge shrinks bandgap of the alloy and thereby redshifting the direct-band absorption edge [25]. Not only that researchers have theoretically shown that the alloy becomes direct bandgap for x > 6% [25], consists of higher saturation velocity [26] and higher mobility [27] than pure Ge. Those noteworthy characteristics have attracted researchers to develop different types of PDs [28-36]. However, those PDs are suitable only for telecommunication applications.

Recently, Pareek et al. have theoretically studied the performance of partially strain-balanced, interband GeSn/SiGeSn single and multiple QWIP at room temperature in MIR region [37-41]. The poor responsivity in the order of ~mA/W [40] and higher dark current of ~μA range [38] may restrict their performance to compete with the existing III-V-based QWIPs. We proposed and theoretically analyzed optical performance of an intersubband (ISB) GeSn/SiGeSn multiple QWIPs (MQWIPs) in MIR region [42]. In

comparison with the previously reported SiGe/Si QWIP, GaAs/AlGaAs QWIP and interband GeSn/SiGeSn QWIP, our proposed ISB GeSn/SiGeSn QWIP showed better optical performance in MIR region [42]. However, in that analysis we have not focused on 3-dB bandwidth (BW) of the device. After finding those motivational results we conducted another study to optimize different structural parameters of the GeSn/SiGeSn QWIP to achieve simultaneously high responsivity and low dark current [43]. From this analysis we found that the optimized ISB QWIP can give > 100 times more detectivity [43] than previously reported SiGe/Si QWIP and interband GeSn/SiGeSn single and multiple QWIP. In addition we calculated BW of the optimally designed QWIP i.e. ~45 GHz. But such a low 3-dB BW may make it unsuitable for recent days' high-speed optical communication system.

Pareek et al. have described different theoretical approaches to increase the BW of interband GeSn/SiGeSn QWIP by increasing the Sn content in the well [38,39] and bias voltage [39,41]. In case of increasing Sn concentration to maintain the strain-balanced condition the barrier width should be reduced. On the other hand, for a fixed number of well the active region thickness reduces that may increase the electric field and thereby reducing the effective barrier height. As a result the increase of Sn concentration increase the dark current due to tunneling and thermionic emission phenomenon [38,39]. Again the increase of bias voltage reduces the effective barrier height. Therefore, the photo-generated carriers can move towards the contact layers with faster rate that may increase the 3-dB BW of the QWIP [39]. However, the increase of bias voltage increases the generation of dark current [38]. Thus, either of these two approaches may help to increase the 3-dB BW of interband QWIP but simultaneously the detectivity may be reduced. Therefore it is important to increase the 3-dB BW of the GeSn/SiGeSn QWIP without compromising its optical property.

In this study the author has designed a new type ISB GeSn/SiGeSn resonant-cavity-enhanced quantum well infrared photodetector (RCE-QWIP) on silicon-on-insulator (SOI) substrate. The top deposited SiO_2 and bottom buried oxide (BOX) layers create vertical cavity effect that may increase the light-matter interaction inside the active layer and thereby the optical responsivity of the QWIP. The author has theoretically shown that the presence of vertical cavity helps to increase the external quantum efficiency and responsivity. Finally, different approaches of increasing 3-dB BW along with high detectivity have been discussed.

The remaining part of the paper is organized as follows, the design of the proposed QWIP is shown in Sec. 2; the theoretical modeling are summarized in Sec. 3; the results are discussed in Sec. 4 and our study is concluded in Sec. 5.

II. Device structure

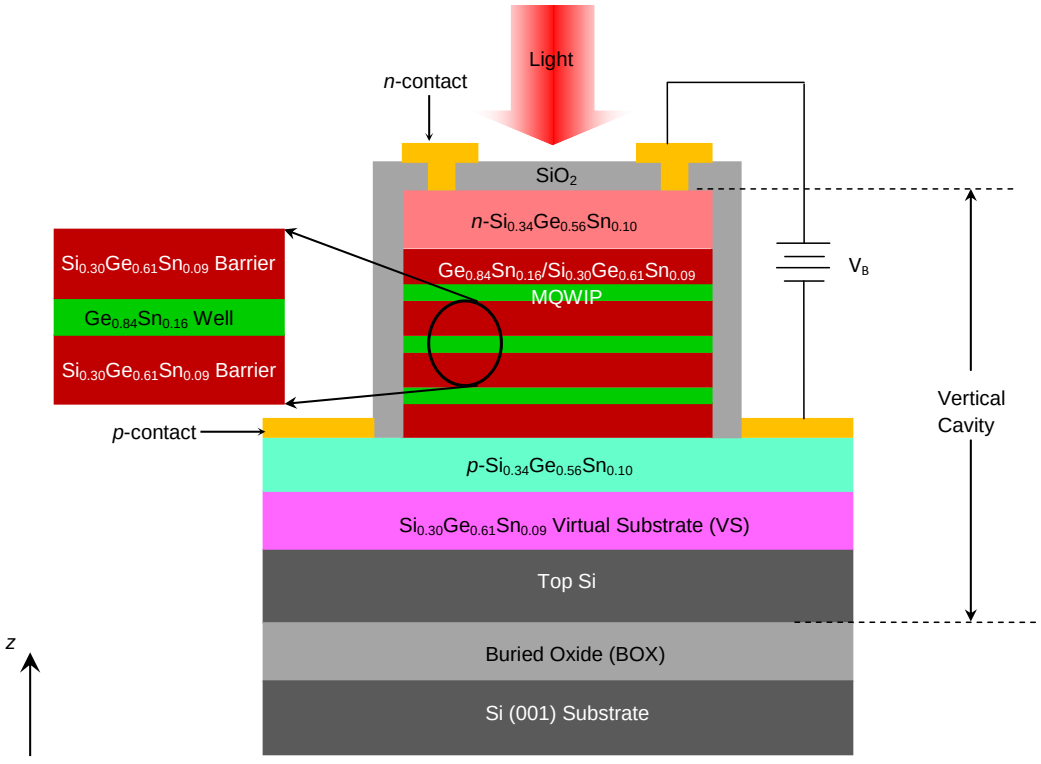

Fig. 1: 2D schematic diagram of the intersubband GeSn/SiGeSn RCE-QWIP on SOI substrate.

Fig. 1 depicts two dimensional (2D) schematic diagram of the proposed ISB GeSn/SiGeSn RCE-QWIP. N number of alternative lower bandgap $Ge_{0.84}Sn_{0.16}$ quantum wells (QWs) and higher bandgaps $Si_{0.30}Ge_{0.61}Sn_{0.09}$ barriers are considered to form active region of the QWIP. We have assumed 20 nm thick barriers and 9 nm thick QWs to ensure negligible carriers' tunneling through the barrier and bound-to-quasicontinuum transition of the carriers inside the wells due to photon absorption respectively [43]. The active region is sandwiched between two heavily doped (~5×10^{18} /cm^3) *p*- and *n*-$Si_{0.34}Ge_{0.56}Sn_{0.10}$ contact layers. The entire structure can be developed on the SOI substrate consists of 1000 nm thick SiO_2 and 2500 nm thick top-Si layer via a lattice-matched $Si_{0.30}Ge_{0.61}Sn_{0.09}$ virtual substrate (VS) to make sure that the barriers are fully strain-relaxed whereas, the wells are compressively strained of ~2.08% [43]. Furthermore as the thickness of QW is lower than the critical thickness (~14 nm), the well is defect-free. In this analysis 77 K and 2 V are assumed as the operating temperature and applied bias voltage. At this low temperature the thermionic emission assisted dark current is very low and at 2 V we can neglect the effect of field assisted tunneling of carriers [43]. On the top of QWIP a 300 nm thick SiO_2 anti-reflection (AR) layer has been deposited to reduce the reflection of incident light from the top surface. The top SiO_2 layer and the BOX layer serve as the top and bottom reflectors that introduce the vertical cavity effect. Therefore, the light which has entered through the AR layer is reflected back from the BOX layer. Thus this multiple-pass technique of the photon energy may increase the light absorption inside the active layer and thereby the optical performance. The applied bias may create a band bending which helps to flow the injected carriers through the active layer producing dark current. On the other hand, in the presence of light energy the photon absorption mechanism helps to raise electrons from bound states to qausicontinuum states inside the wells [43]. The movement of those photo-generated electrons towards contact layers produce photocurrent. Thus the total current flow through the QWIP is the sum of dark current and photocurrent.

III. Theoretical Analysis

In this section, we have described the theoretical analysis to study the performance of the proposed GeSn/SiGeSn QWIP on SOI in MIR, including the absorption coefficient, external quantum efficiency (EQE), optical responsivity, 3-dB BW, dark current, dark current noise and detectivity. Due to the lack of experimental data for GeSn and SiGeSn alloys, the material parameters of GeSn and SiGeSn alloys used in this study are obtained from Si, Ge and α–Sn [42,43].

3.1 Absorption Coefficient

In this study we have assumed the growth direction of GeSn/SiGeSn QWIP is along z-axis. Thus the ISB transition only occurs by absorbing transverse magnetic (TM) polarized light because ISB optical dipole moment contains only z-component. On the contrary, as x- and y-components of the ISB dipole moment is zero, the ISB transition cannot take place by absorbing transverse electric (TE) polarized light. The absorption coefficient of the QWIP can be evaluated by [44,45],

$$\alpha(\hbar\omega) = \left(\frac{\omega}{n_r c\varepsilon_0}\right)\frac{|\mu_{21}|^2(\Gamma/2)}{(E_2 - E_1 - \hbar\omega)^2 + (\Gamma/2)^2}\left(\frac{m_e^*}{\pi\hbar^2 L_W}\right)(E_2 - E_1) \quad (1)$$

where ω denotes the angular frequency of the incident photon energy, n_r is the refractive index (R.I.) of the material, c represents the velocity of light in vacuum, ε_0 is the free space permittivity, Γ (= 20 meV) is the line width, m_e^* is the electron effective mass, E_1 and E_2 are the bounded ground state and first excited state subband energy, L_W denotes the thickness of well and μ_{21} is the ISB dipole moment which can be expressed as, $\mu_{21} = \langle\varphi_2|ez|\varphi_1\rangle$, φ_Ω represents the wave function of Ω-energy state.

3.2 External Quantum Efficiency

The EQE of a conventional QWIP can be calculated as [42],

$$\eta_{QWIP} = (1 - R_1)[1 - \exp(-\alpha L_W N)] \quad (2)$$

where R_1 is the reflectivity of the top surface [42], α is the absorption coefficient and N is the number of well. The EQE of a RCE-QWIP can be evaluated by,

$$\eta_{RCE-QWIP} = \frac{[1 + R_2\exp(-\alpha L_W N)](1 - R_1)\,[1 - \exp(-\alpha L_W N)]}{1 - 2\sqrt{R_1 R_2}\exp(-\alpha L_W N)\cos(2\beta L_C + \Psi_1 + \Psi_2) + R_1 R_2\exp(-2\alpha L_W N)} \quad (3)$$

where R_2 is the reflectivity of the BOX layer, L_C is the cavity length, Ψ_1 and Ψ_2 represent the phase shifts introduced by the top and bottom SiO_2 and BOX layers respectively. The propagation constant β is calculated by, $\beta = \frac{2\pi n_r}{\lambda}$ with wavelength λ.

3.3 Escape probability, photoconductive gain and Optical Responsivty,

The escape probability (p_e) denotes the fraction of photo-generated carriers which escape from the QW and produce photocurrent. Therefore, if n_p, n_c and n_e denote the concentration of total photo-generated carriers,

captured carriers in the neighbourhood QWs and escaped carriers respectively, the escape probability can be expressed as,

$$p_e = \frac{n_e}{n_P} = 1 - \frac{n_c}{n_P} = 1 - p_c \quad (4)$$

where p_c is the capture probability of the photo-generated carriers inside the QWs.
The photoconductive gain (g_{ph}) can be calculated as [42],

$$g_{ph} = \left(\frac{1 - p_C}{p_C}\right)\frac{1}{N} \quad (5)$$

where N is the number of QW. From Eqs. (4) and (5) we can express g_{ph} in terms of p_e as,

$$g_{ph} = \left(\frac{p_e}{1 - p_e}\right)\frac{1}{N} \quad (6)$$

Again g_{ph} can be expressed in terms of photo-generated carriers' lifetime (τ) as [42],

$$g_{ph} = \frac{v(F)\tau}{NL_P} \quad (7)$$

where L_P is the single period of QWIP that can be measured by, $L_P = L_W + L_B$ with barrier thickness L_B, v(F) is the carriers' drift velocity which can be calculated as [42],

$$v(F) = \frac{\mu F}{\sqrt{1 + (\mu F/v_s)^2}} \quad (8)$$

where μ is the carriers' mobility, F is the applied electric field and v_s denotes the carriers' saturation velocity.
Then from Eqs. (6) and (7) we can express the escape probability in terms of carriers' lifetime as,

$$p_e = \left[\frac{v(F)\tau}{L_P + v(F)\tau}\right] \quad (9)$$

The optical responsivity of a QWIP can be calculated by [42],

$$R_\lambda = \left(\frac{e\eta g_{ph}}{hc}\right)\lambda \quad (10)$$

where e is the electronic charge, η is the EQE and h denotes the Planck's constant.
From Eq. (6) and (10) we can write,

$$R_\lambda = \frac{1}{N}\left(\frac{e\eta\lambda}{hc}\right)\left(\frac{p_e}{1 - p_e}\right) \quad (11)$$

The responsivity can be expressed in terms of carriers' lifetime as [42],

$$R_\lambda = \left(\frac{e\eta\lambda}{hc}\right)\left(\frac{v(F)\tau}{NL_P}\right) \quad (12)$$

The frequency dependent responsivity of QWIP can be calculated using empirical expression as [10],

$$R_\lambda(\omega) = R_{0\lambda}\frac{2}{i\omega\tau_t(N+1)}\frac{e^{i\omega\tau_t} - 1}{[1 - (1 - p_e)e^{i\omega\tau_t}]^2} \times \left[(1 - p_e)^{N+1}e^{i\omega\tau_t(N+1)} - (1 - p_e)(N+1)e^{i\omega\tau_t} + N\right] \quad (13)$$

where τ_t is the electron transit time i.e. $\tau_t = (N + 1 - t/v_s)$ with t = 1,2,3...N [10], $R_{0\lambda} = e\sigma\Sigma_0/2\hbar\Omega$, σ is the photo-excitation cross-section, $\hbar\Omega$ represents the incident photon energy and Σ_m is the electron-sheet concentration in m^{th} QW in the bound state.

3.4 Dark Current and Dark Current Noise

The dark current (I_{dark}) of QWIP can be calculated as [43,45],

$$I_{dark} = eA_d n(F)v(F) \quad (14)$$

where A_d represents cross-sectional area of detection and n(F) is thermally-generated carriers [43].
The noise is an important parameter that can affect the operation of MIR PDs. Among different noise components we can neglect the effect of Flicker (1/f) noise and Johnson-Nyquist (thermal) noise. The Flicker noise only governs at low frequency (< 1 MHz) operation [46] whereas the thermal noise is dominating at high operating temperature [43]. Therefore, only dark current shot noise component plays important role in this analysis. The dark current shot noise can be calculated by [19],

$$\langle i_n^2 \rangle = \sqrt{4eI_{dark}\, g_n \Delta f} \quad (15)$$

where g_n is noise gain that can be calculated as [19], $g_n = g_{ph}(1 - p_c/2)$ and Δf is the BW [19].

3.5 Detectivity

The detectivity (D^*) of the QWIP can be calculated by [43],

$$D^* = \frac{R_\lambda\sqrt{A_d\Delta f}}{\sqrt{\langle i_n^2 \rangle}} \quad (16)$$

IV. Results and Discussions

In this section we have first investigated the reflectivity of the SOI substrate and then we have shown a comparative study of the EQE and optical responsivity spectra of the optimally designed GeSn/SiGeSn QWIP on Si [43] and the proposed model. Later we have discussed different theoretical approaches to increase the 3-dB BW without decreasing the detectivity.

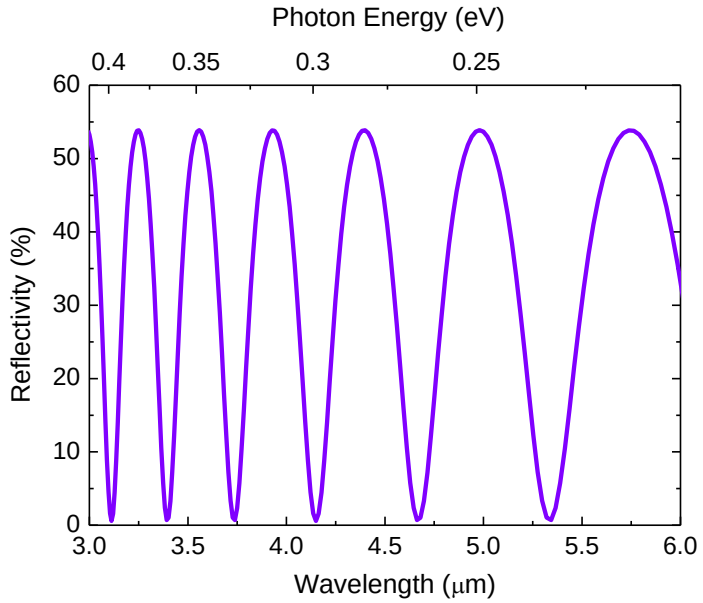

Fig. 2: Reflectivity of the SOI substrate.

We have calculated the reflectivity of the SOI using transfer matrix method (TMM). In Fig. 2 the reflectivity shows a clear oscillatory nature. To calculate the reflectivity of the SOI substrate, the reflectances of Si substrate, Oxide layer and top Si layer have been taken into consideration. The oscillatory nature of reflectivity gives a clear evidence of the interference between those layers. The peak reflectivity can be achieved ~55%. In mid infrared region both SiO_2 and Si layers act as transparent, therefore the responsivity is free from any additional absorption loss introduced by SOI substrate.

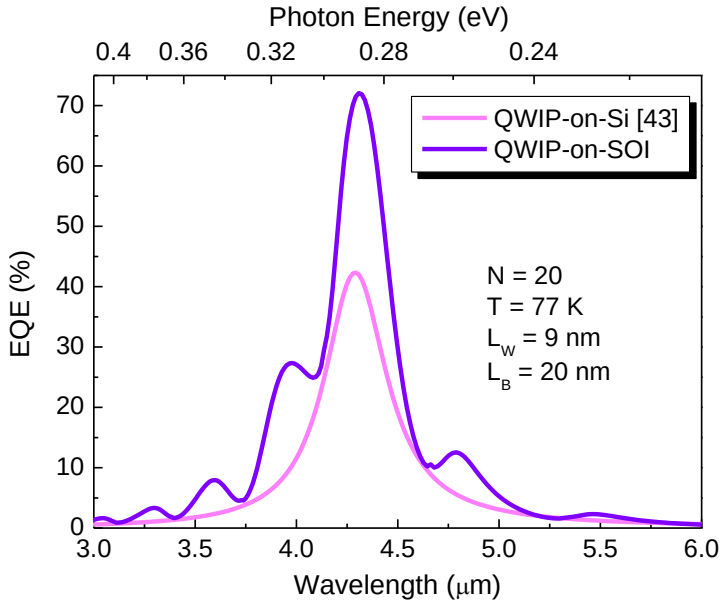

Fig. 3: Variation of Calculated EQE as a function of wavelength (Photon Energy) of GeSn/SiGeSn QWIP-on-Si and QWIP-on-SOI.

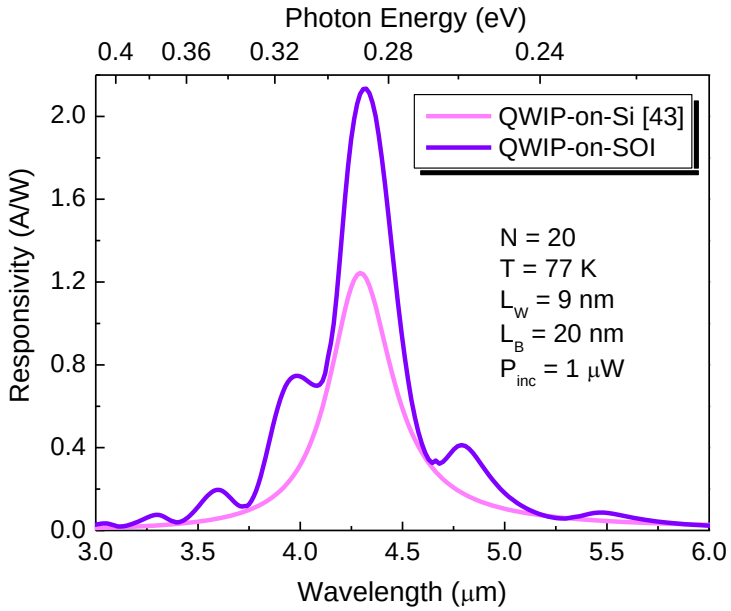

Fig. 4: Variation of Calculated responisivity against wavelength (Photon Energy) of GeSn/SiGeSn QWIP-on-Si and QWIP-on-SOI.

The EQE and optical responsivity have been calculated using Eqs. (2)-(3) and (10) respectively. Fig. 3 and 4 depict the variation of EQE and optical responsivity as a function of optical wavelength (Photon energy) respectively. In the QWIP-on-SOI model the top deposited SiO_2 and the bottom BOX layers create a vertical cavity. Due to the resonating effect at constructive interference more amount of photon energy can be absorbed inside the active region of QWIP-on-SOI than QWIP-on-Si. Thus, both the EQE and responsivity increase ~170% than the conventional QWIP-on-Si. The peak EQE and responsivity achieve due to the ISB transition of the carriers in conduction band for both the QWIPs. Moreover, for the QWIP-on-SOI model the EQE and optical responsivity give several small peaks. The EQE and responsivity of QWIP-on-SOI depend on the reflectivity of SOI substrate which shows an oscillatory nature as depicted in Fig. 2. At the peak reflectivity (~55%) more amount of light can be reflected from the BOX layer that may increase the light-matter interaction and thereby the EQE and responsivity.

To give a clear view of the resonating effect we have used finite element method (FEM) to show the simulated optical field distribution inside the QWIP-on-Si and QWIP-on-SOI in Fig. 5. In Fig. 5(a) inspite of strong reflection of the incident photon energy at air-SiO_2 interface a small amount of light can enter inside the QWIP. But due to smaller difference of RIs between $Si_{0.30}Ge_{0.61}Sn_{0.09}$ VS (n~3.95) and Si substrate (n~3.45) a poor optical confinement occurs. As a result, the light intensity is very weak at the active region. On the other hand, for the QWIP-on-SOI model depicted in Fig. 5(b), the absorbed light can pass multiple times inside the QWIP because of the reflection between air-SiO_2 and BOX-Si interfaces. The higher contrast of RIs between SiO_2 (n~1.45) and Si (n~3.45) creates optical confinement that may develop standing wave pattern. Therefore, the intensity of the light increases at the active region by ~165% than the conventional QWIP-on-Si structure. This simulated result gives a strong agreement with our calculated data that the EQE and optical responsivity of the QWIP can be increased by using SOI substrate instead of Si. In the presence of TM polarized light the simulated electric field (E_Z) distribution inside the QWIP-on-Si and QWIP-on-SOI models are illustrated in Fig. 6.

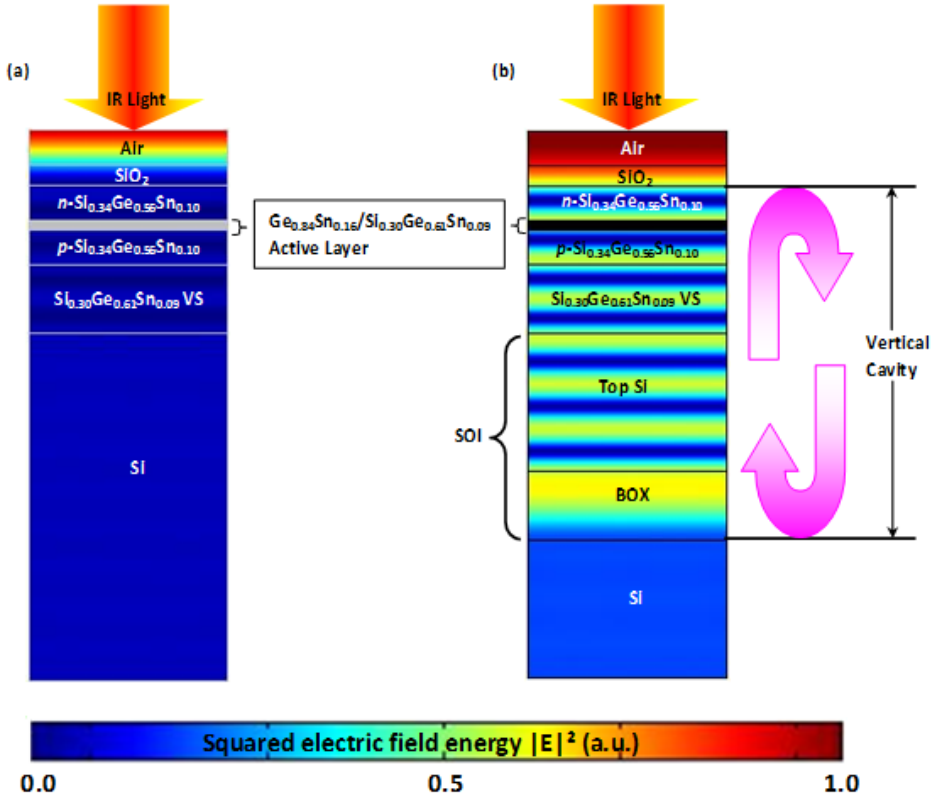

Fig. 5: Simulated optical field distribution of GeSn/SiGeSn (a) QWIP-on-Si and (b) QWIP-on-SOI in MIR region.

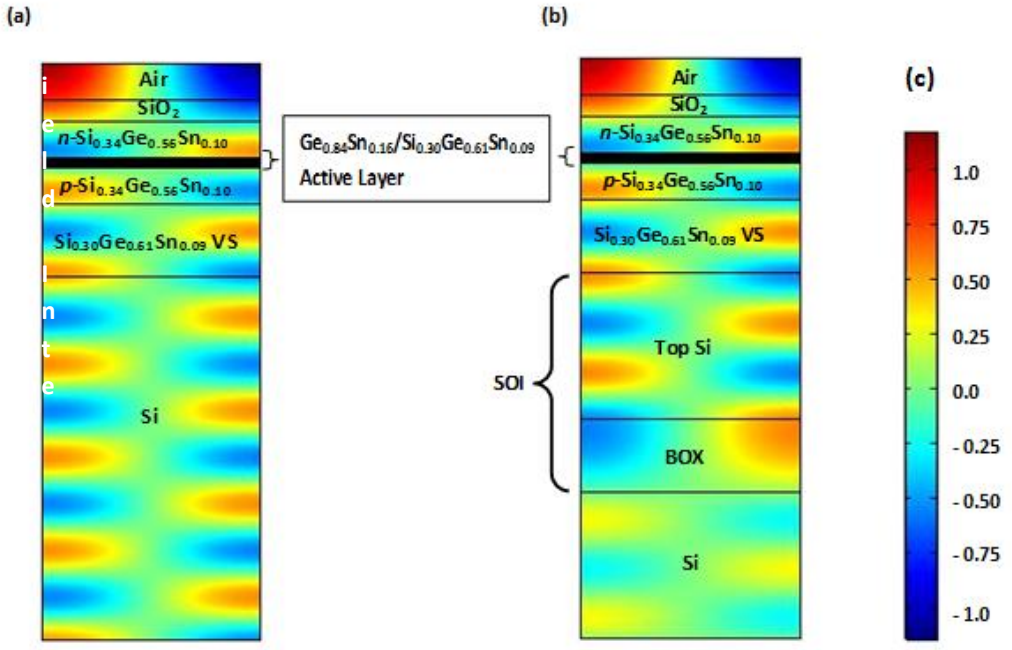

Fig. 6: Simulated electric field distribution of GeSn/SiGeSn (a) QWIP-on-Si and (b) QWIP-on-SOI in MIR region in the presence of TM polarized light. (c) Electric field distribution in arbitrary unit.

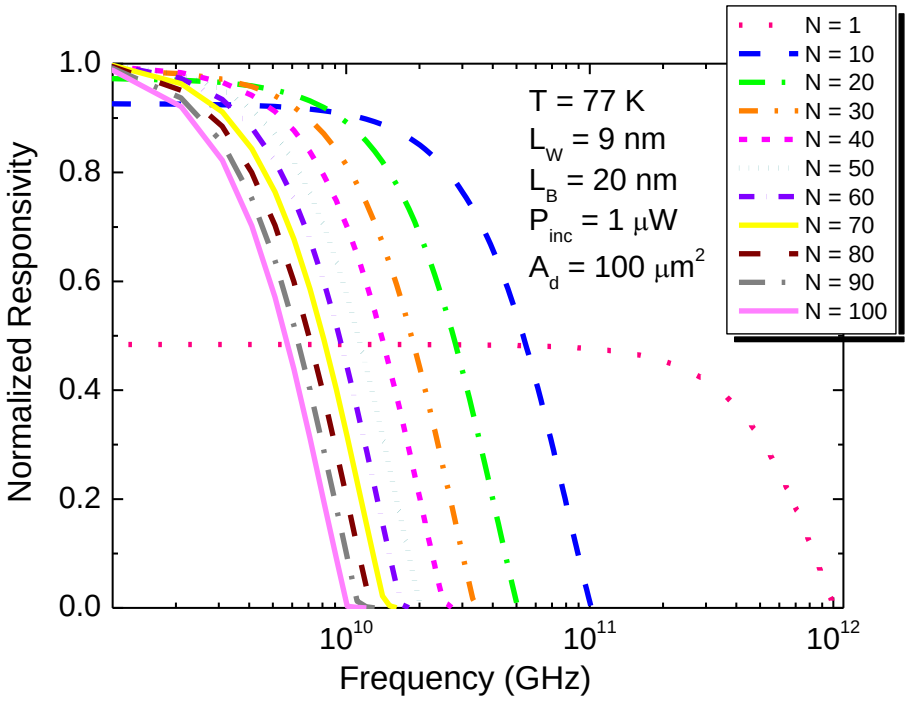

Fig. 7: Variation of normalized responsivity with operating frequency for different number of well.

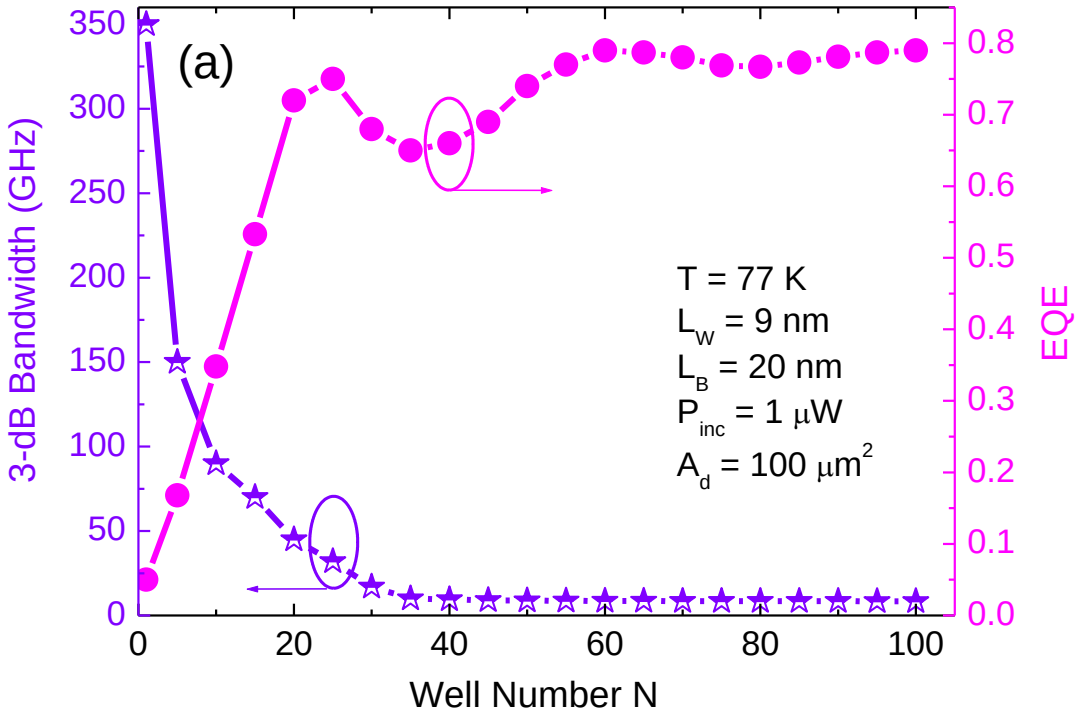

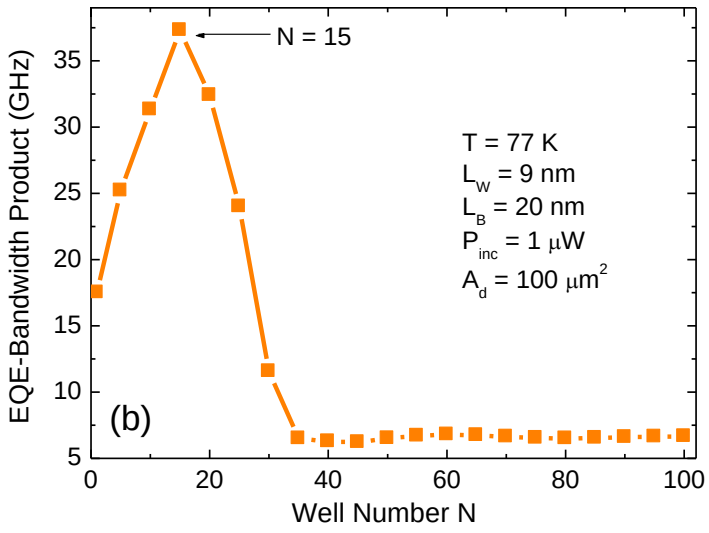

Fig. 8: (a) Variation of 3-dB Bandwidth and EQE as a function of well number. (b) Variation of EQE-Bandwidth product against well number.

From Fig. (3) and (4) it can be said that the use of SOI substrate instead of Si the EQE and responsivity increase and thereby the detectivity. Now, in this section we have discussed about several approaches to increase the 3-dB BW of the GeSn/SiGeSn QWIP without reducing the detectivity. Using Eq. (13) we have calculated normalized responsivity of the GeSn/SiGeSn RCE-QWIP and plotted against operating frequency in Fig. 7 for different well number. From this figure it is clearly observed that the increase of well number decreases the 3-dB BW. Thus QWIP with lesser number of QW can give high 3-dB BW. But the reduction of well number may reduce the active region area and consequently the EQE decreases. Therefore, to get a clear view of the effect of well number on the 3-dB BW as well as its EQE we have plotted their variation in Fig. 8(a). The decrease of well number reduces the active region thickness. Thus, the photo-generated carriers take smaller time to reach the contacts. Therefore the 3-dB BW increases. On the other hand, the smaller active region can absorb a small amount of photon energy which leads to decrease the EQE of the QWIP. From this figure, it can be stated that for single QW the device can produce ~350 GHz BW but the corresponding EQE is only ~0.05. Thus we cannot consider single well to get highest 3-dB BW with such a small EQE. From this analysis we have found there is a trade-off between EQE and 3-dB BW. Therefore we have calculated EQE-BW product to obtain high 3-dB BW and simultaneously high EQE. Fig. 8(b) shows the variation of the EQE-BW product against QW number. The peak EQE-BW product has been obtained for N = 15 with 70 GHz BW and EQE of 0.53. From our previous study we have found that for ISB GeSn/SiGeSn QWIP-on-Si 20 is the optimum well number for which it can give highest detectivity of 3.47×10^{12} cm·Hz$^{1/2}$W^{-1} at 2 V with 45 GHz BW [43], whereas the QWIP-on-SOI model for 15 number of wells can give detectivity of 6.24×10^{12} cm·Hz$^{1/2}$W^{-1} at 2 V. Therefore, in case of the proposed structure the reduction of number of well increases the 3-dB BW by ~56% and due to resonating effect the detectivity also increases by ~80% than the optimized ISB GeSn/SiGeSn QWIP [43].

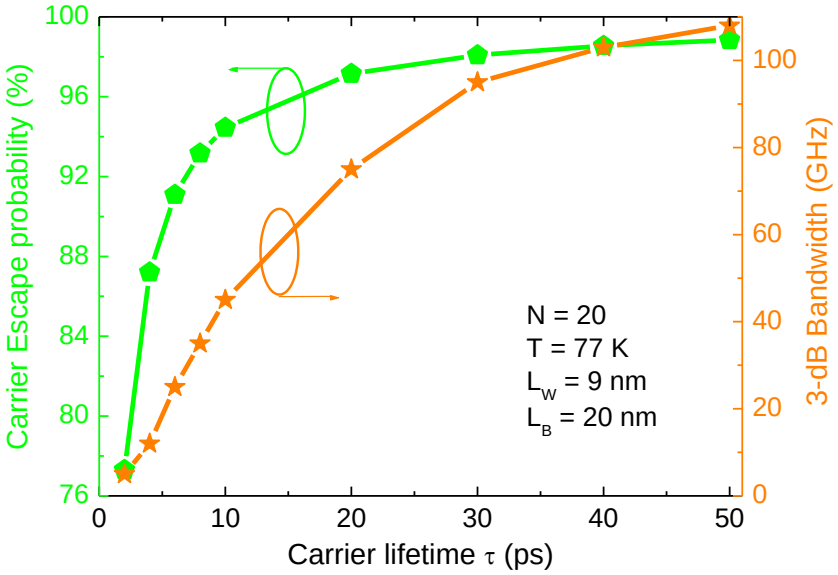

Fig. 9: Variation of carrier escape probability and 3-dB BW as a function of carrier lifetime.

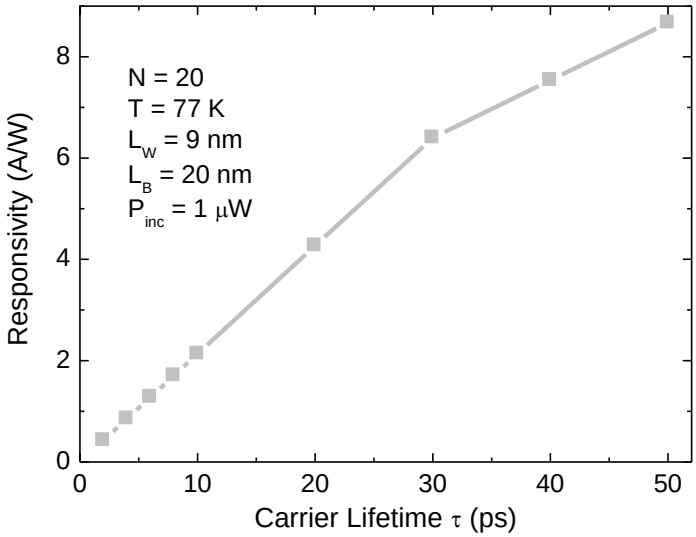

Fig. 10: Variation of responsivity as a function of carrier lifetime.

Figure 9 exhibits the variation of carriers' escape probability and 3-dB BW as a function of carrier lifetime calculated using Eqs. (9) and (13) respectively for a fixed number of QW. The increase of carrier lifetime helps to escape more numbers of carriers that are generated due to photon absorption from the QWs and move towards the contacts. Thus the escape probability increases with increase of carriers' lifetime and beyond 30 ps it shows a saturation trend where almost more than 96% of the photo-generated carriers escape from the well. On the other hand, as the photo-generated carriers with larger lifetime move faster towards the contacts before capturing to the neighbouring well, the speed of the QWIP increases and thereby the 3-dB BW. Therefore, the 3-dB BW also increases with increase of the carrier lifetime. The effect of carrier lifetime on the optical responsivity has been calculated using Eq. (12) and plotted in Fig. 10. As the escape rate of photo-generated carriers increases with increase of carrier lifetime as shown in Fig. 9, the concentration of photo-generated carriers increase at the contacts and thereby the optical responsivity. These results illustrate that the 3-dB BW and responsivity both increase with increase of carrier lifetime from 2 ps to 30 ps very rapidly and beyond that they increase with slower rate as most of the photo-generated carriers (> 96%) whose lifetime is

more than 30 ps escape from the well. So it can be stated that higher carrier lifetime may yield higher 3-dB BW and responsivity. The carrier lifetime may be increased by using chemical mechanical polishing technique which may develop a defect-free structure and reduce different nonradiative recombination processes such as Shockley-Read-Hall, surface recombination etc. However, it cannot be possible to make a complete defect-free structure with free from the nonradiative recombination centres. Thus we cannot increase the carriers' lifetime infinitely. Therefore, we have considered 30 ps as the carrier lifetime for which our proposed model can achieve 3dB-BW and detectivity of 95 GHz and 17.6×10^{12} cm·$Hz^{1/2}W^{-1}$ at 2 V respectively which are more than 2 and 5 times of the BW and detectivity obtained from the optimally designed GeSn/SiGeSn QWIP-on-Si [43]. In Table 1 we have given our estimated results along with the optimally designed GeSn/SiGeSn QWIP.

Table 1: Calculated 3-dB BW and detectivity of our proposed GeSn/SiGeSn QWIP on SOI model.

Parameters	Device	Peak Detectivity (cm·$Hz^{1/2}W^{-1}$) at 2 V	3-dB BW (GHz)
N = 20, τ = 10 ps	QWIP-on-Si	3.47×10^{12} [43]	45 [43]
N = 15, τ = 10 ps	QWIP-on-SOI	6.24×10^{12}	70
N = 20, τ = 30 ps	QWIP-on-SOI	17.6×10^{12}	95

V. Conclusion

In this study we have theoretically demonstrated the performance of an ISB GeSn/SiGeSn QWIP on SOI substrate in MIR region. The EQE and responsivity both increase due to the presence of vertical cavity effect than the conventional QWIP on Si. Moreover, in this analysis we have theoretically investigated different approaches including reduction of well number and increase of carrier lifetime to increase the 3-dB BW without decreasing the detectivity. In both the cases we have found that this proposed QWIP can give higher 3-dB BW and simultaneously higher detectivity than the previously reported ISB GeSn/SiGeSn QWIP. Due to its monolithic integrability on same Si chip, Si-based CMOS compatibility, high 3-dB BW along with high detectivity the proposed GeSn/SiGeSn RCE-QWIP is an encuraging device for high-performance photodetection in MIR applications.

References

[1]. P. Pareek, R. Ranjan, S. K. Pandey, J. K. Mishra, A. K. Kushwaha, "Performance Comparison of Tin based Group IV SQWIP and MQWIP in Dark Conditions," *Nanophotonics VIII*, *Proc. of SPIE*, **11345**, p. 113452A, 2020.

[2]. S. D. Gunapala, J. S. Park, G. Sarusi, L. True_Lon, J. K. Liu, P. D. Maker, "15μm 128×128 GaAs/$Al_xGa_{1-x}As$ quantum well infrared photodetector focal plane array camera," *IEEE Trans. Electron. Dev.* **44**, pp. 45-50, 1997.

[3]. S. D. Gunapala, S. V. Bandara, A. Singh, J. K. Liu, B. Rafol, "640×486 long wavelength two color GaAs/$Al_xGa_{1-x}As$ quantum well infrared photodetector (QWIP) focal plane array camera," *IEEE Trans. Electron. Dev.* **47**, pp. 963-971, 2000.

[4]. A. Rogalski, "Infrared detectors: an overview," *Infrared Phys. Tech.* **43**, pp. 187-202, 2002.

[5]. V. Gueriaux, N. de Brierel'Isle, A. Berurier et al., "Quantum well infrared photodetectors: present and future," *Opt. Engg.* **50**, p. 061013, 2011.

[6]. C. Downs, T. E. Vandervelde, "Progress in infrared photodetectors Since 2000," *Sensors* **13**, pp. 5054-5098, 2013.

[7]. B. F. Levine, A. Zussman, S. D. Gunapala, M. T. Asom, J. M. Kuo, W. S. Hobson, "Photoexcited escape probability, optical gain and noise in quantum well infrared photodetectors," *J. Appl. Phys.* **72**, pp. 4429-4443, 1992.

[8]. B. F. Levine, "Device physics of quantum well infrared photodetectors," *Semicond. Sci. Technol.* **8**, pp. S400-S405, 1993.

[9]. V. Ryzhii, "Characteristics of quantum well infrared photodetectors," *J. Appl. Phys.* **81**, pp. 6442-6448, 1997.

[10]. V. Ryzhii, I. Khmyrova, and M. Ryzhii, "Impact of transit time and capture effects on high-frequency performance of multiple quantum well infrared photodetectors," *IEEE Trans. Electron Dev.* **45**, pp. 293-298, 1998.

[11]. V. Ryzhii, "High-frequency performance of single well infrared photodetectors at high power densities," *IEEE Trans. Electron Dev.* **45**, pp. 1797-1803, 1998.

[12]. T. Mei, H. Li, G. Karunasiri, W. J. Fan, D. H. Zhang, S. F. Yoon, K. H. Yuan, "Normal incidence silicon doped p-type GaAs/AlGaAs quantum well infrared photodetector on (111) Å substrate," *Infrared Phys. & Tech.* **50**, pp. 119-123, 2007.

[13]. S. D. Gunapala, D. R. Rhiger, C. Jagadish, "Advances in Infrared Photodetectors," vol. 84, 1st edn., *Academic Press, Cambridge*, 2011.

[14]. S. D. Gunapala, S. V. Bandara, J. K. Liu, J. M. Mumolo, , Sir B. Rafol, D. Z. Ting, A. Soibel, C. Hill, "Quantum Well Infrared Photodetector Technology and Applications," *IEEE J. Sel. Top. Quantum Electron*. **20**, p. 3802312, 2014.

[15]. G. Q. Lo, K. W. Ang, T. Y. Liow et al., "Silicon photonics technologies for monolithic electronic-photonic integrated circuit," *ECS Trans.* **28**, pp. 3-11, 2010.

[16]. P. Kruck, M. Helm, T. Fromherz, G. Bauer, "Medium-wavelength, normal incidence, p-type Si/SiGe quantum well infrared photodetector with background limited performance up to 85 K," *Appl. Phys. Lett.* **69**, pp. 3372-3374, 1996.

[17]. M. A. Gadir, P. Harrison, R. A. Soref, "Responsivity of quantum well infrared photodetector at terahertz detection wavelength," *J. Appl. Phys.* **91**, pp. 5820-5825, 2002.

[18]. D. Heqing, L. Guijang, L. Hongkai, L. Cheng, C. Songyan and Y. Jinzhong, "An Energy Band Design for p-type Tensile Strained Si/SiGe Quantum Well Infrared Photodetectors," *J. Semicond.* **29**, pp.785-788, 2008.

[19]. P. Rauter, T. Fromherz, C. Falub, D. Grutzmacher, G. Bauer, "SiGe quantum well infrared photodetectors on pseudosubstrate," *Appl. Phys. Lett*. **94**, p. 08115, 2009.

[20]. H. Durmaz, P. Sookchoo, X. Cui, R. B. Jacobson, D. E. Savage, M. G. Lagally, R. Paiella, "SiGe Nanomembrane Quantum-Well Infrared Photodetectors," *ACS Photonics* **3**, pp. 1978-1985, 2016.

[21]. J. Aberl, M. Brehm, T. Fromherz, J. Schuster, J. Frigerio, and P. Rauter, "SiGe quantum well infrared photodetectors on strained-silicon-on-insulator," *Opt. Express* **27**, pp. 32009-32018, 2019.

[22]. A. V. G. Chizmeshy, C. Ritter, J. Tolle, C. Cook, J. Menendez, J. Kouvetakis, "Fundamental studies of $P(GeH_3)_3$, $As(GeH_3)_3$, and $Sb(GeH_3)_3$: practical n-dopants for new group IV semiconductors," *Chem. Mater.* **18**, pp. 6266-6277, 2006.

[23]. R. Roucka, J. Xie, J. Kuovetakis, J. Mathews, V. D'Costa, J. Menendez, J. Tolle, S. Q. Yu, "$Ge_{1-y}Sn_y$ photoconductor structures at 1.55 µm: from advanced materials to prototype devices," *J. Vac. Sci. Technol. B.* **26**, pp. 1952-1959, 2008.

[24]. J. P. Gupta, N. Bhargava, S. Kim, T. Adam, J. Kolodzey, "Infrared electroluminescence from GeSn heterojunction diodes grown by molecular beam epitaxy," *Appl. Phys. Lett.* **102**, p. 251117, 2013.

[25]. G. –E. Chang, S. –Q. Yu, J. Liu, H. H. Cheng, R. A. Soref, G. Sun, "Achievable performance of uncooled homojunction GeSn mid–infrared photodetectors," *IEEE J. Sel. Quantum Electron*. **28**, p. 3800611, 2022.

[26]. S. Ghosh, R. Bansal, G. Sun, R. A. Soref, H. –H. Cheng, G. –E. Chang, "Design and Optimization of GeSn Waveguide Photodetectors for 2-µm Band Silicon Photonics," *Sensors* **22**, p. 3978, 2022.

[27]. R. Soref, "Mid-Infrared Photonics," in *Optical Fiber Communication Conference* (*OFC*), p. W4A.4, 2015.

[28]. Y. Dong, W. Wang, X. Xu, X. Gong, D. Lei, Q. Zhou, Z. Xu, W. KhaiLoke, S. –F. Yoon, G. Liang, Y. –C. Yeo, "Germanium-Tin on Si Avalanche Photodiode: Device Design and Technology Demonstration," *IEEE Trans. Electron Dev.*, **62**, pp. 128-135, 2015.

[29]. S. Ghosh, K. –C. Lin, C. –H. Tsai, H. Kumar, Q. Chen, L. Zhang, B. Son, C. S. Tan, M. Kim, B. Mukhopadhyay, and G. –E. Chang, "Metal-Semiconductor-Metal GeSn Photodetectors on Silicon for Short-Wave Infrared Applications," *Micromachines*, vol. 11, p. 795, 2020.

[30]. H. Wang, J. Zhang, G. Zhang, Y. Chen, Y. C. Huang,; X. Gong, "High–speed and high–responsivity p–i–n waveguide photodetector at a 2µm wavelength with a $Ge_{0.92}Sn_{0.08}$/Ge multiple–quantum–well active layer," *Opt. Lett.* **46**, pp. 2099–2102, 2021.

[31]. S. Ghosh, B. Mukhopadhyay, G. –E. Chang, "Design and Analysis of GeSn-Based Resonant-Cavity-Enhanced Photodetectors for Optical Communication Applications," *IEEE Sensors J*. **20**, pp. 7801-7809, 2020.

[32]. S. Ghosh, H. Kumar, B. Mukhopadhyay, G. –E. Chang, "Design and modeling of high–performance DBR–based resonant–cavity–enhanced GeSn photodetector for fiber–optic telecommunication networks," *IEEE Sens. J.* **21**, pp. 9900–9908, 2021.

[33]. G. –E. Chang, R. Basu, B. Mukhopadhyay, P. K. Basu, "Design and Modeling of GeSn–Based Heterojucntion Phototransistors for Communication Applications," *IEEE J. Sel. Quantum Electron.* **22**, p. 8200409, 2016.

[34]. S. Ghosh, B. Mukhopadhyay, G. Sen, P. K. Basu, "Study of Si–Ge–Sn based Heterobipolar Phototransistor (HPT) Exploiting Quantum Confined Stark Effect and Franz Keldysh Effect with and Without Resonant Cavity," *Phys. E* **106**, pp. 62–67, 2019.

[35]. W. -T. Hung, D. Barshilia, R. Basu, H. H. Cheng, G. –E. Chang, "Silicon–based High–responsivity GeSn Short–wave Infrared Heterojunction Phototransistors with a Floating Base," *Opt. Lett.* **45**, pp. 1088–1091, 2020.

[36]. S. Ghosh, "Comparative Study of Si–Ge–Sn Resonant Cavity Enhanced Heterojunction Bipolar Phototransistor under Quantum Confined Stark Effect and Franz Keldysh Effect at 1.55 µm," *IOSR J. Elec. Comm. Eng*. 17, pp. 1–10, 2022.

[37]. P. Pareek, M. K. Das, "Theoretical analysis of direct transition in SiGeSn/GeSn strain balanced QWIP," *Opt. Quant. Electron.*, **48**, pp. 1-11, 2016.

[38]. P. Pareek, M. K. Das, S. Kumar, "Theoretical analysis of tin incorporated group IV alloy based QWIP," *Superlatt. And Microstruct.*, **107**, pp. 56-68, 2017.

[39]. P. Pareek, M. K. Das, S. Kumar, "Numerical analysis of SiGeSn/GeSn interband quantum well infrared photodetector," *Opto-Electron. Review* **26**, pp. 149-157, 2018.

[40]. P. Pareek, M. K. Das, S. Kumar, "Responsivity calculation of group IV based inter band MQWIP," *J. Comput. Electron.*, **17**, pp. 319-328, 2018.

[41]. P. Pareek, R. Ranjan, M. K. Das, "Numerical analysis of tin incorporated group IV alloy based MQWIP," *Opt. Quant. Electron.*, **50**, p. 179, 2018.

[42]. S. Ghosh, B. Mukhopadhyay, G. Sen, P. K. Basu, "Performance Analysis of GeSn/SiGeSn Quantum Well Infrared Photodetector in terahertz wavelength region", *Phys. E*, **115**, p. 113692, 2020.

[43]. S. Ghosh, A. Bhattacharyya, G. Sen, B. Mukhopadhyay, "Optimization of different structural parameters of GeSn/SiGeSn Quantum Well Infrared Photodetectors (QWIPs) for low dark current and high responsivity," *J. Comp. Electron.* 20, pp. 1224–1233, 2021.

[44]. S. B. Adamu, I. A. Faragai, U. Ibrahim, "Optical Absorption in GaAs/AlGaAs Quantum Well due to Transitions," *Progress in Phys.*, **15**, pp. 23-25, 2019.

[45]. S. L. Chuang, "Physics of Optoelectronic Devices," *A Wiley-Interscience Publication.*

[46]. H. Kumar, R. Basu, G. –E. Chang, "Impact of Temperature and Doping on the Performance of $Ge/Ge_{1-x}Sn_x/Ge$ Heterojunction Phototransistors," *IEEE Photon. J*. **12**, p. 6801814, 2020.

Soumava Ghosh. "Study the performance of GeSn/SiGeSn quantum well infrared photodetector on silicon-on-insulator in mid-infrared region." *IOSR Journal of Electronics and Communication Engineering (IOSR-JECE)* 17(5), (2022): pp 15-26.